⌘ *Author's Choice*

THE JOURNAL OF BIOLOGICAL CHEMISTRY VOL. 287, NO. 15, pp. 12142–12151, April 6, 2012

Cytosolic Ni(II) Sensor in Cyanobacterium

NICKEL DETECTION FOLLOWS NICKEL AFFINITY ACROSS FOUR FAMILIES OF METAL SENSORS[*S]

Received for publication, December 28, 2011, and in revised form, February 20, 2012 Published, JBC Papers in Press, February 22, 2012, DOI 10.1074/jbc.M111.338301

Andrew W. Foster[‡§], **Carl J. Patterson**[‡], **Rafael Pernil**[‡], **Corinna R. Hess**[‡], **and Nigel J. Robinson**[‡1]

From the [‡]*Biophysical Sciences Institute, Department of Chemistry, School of Biological and Biomedical Sciences, University of Durham, Durham DH1 3LE, United Kingdom and the* [§]*Institute for Cell and Molecular Sciences, Medical School, Newcastle University, Newcastle upon Tyne NE2 4HH, United Kingdom*

Background: The function of CsoR/RcnR-like protein InrS was unknown.
Results: InrS and CsoR metal complexes have similar spectra, but InrS senses nickel not copper.
Conclusion: InrS detects cytosolic nickel with tighter K_D than the other metal sensors of the cell.
Significance: InrS might be exploited to optimize hydrogenase Ni(II) supply, and this study shows how metal specificity can be a shared function of a set of metal sensors.

Efflux of surplus Ni(II) across the outer and inner membranes of *Synechocystis* PCC 6803 is mediated by the Nrs system under the control of a sensor of periplasmic Ni(II), NrsS. Here, we show that the product of ORF *sll0176*, which encodes a CsoR/RcnR-like protein now designated InrS (for internal nickel-responsive sensor), represses *nrsD* (NrsD is deduced to efflux Ni(II) across the inner membrane) from a cryptic promoter between the final two ORFs in the *nrs* operon. Transcripts initiated from the newly identified *nrsD* promoter accumulate in response to nickel or cobalt but not copper, and recombinant InrS forms specific, Ni(II)-inhibited complexes with the *nrsD* promoter region. Metal-dependent difference spectra of Ni(II)- and Cu(I)-InrS are similar to Cu(I)-sensing CsoR and dissimilar to Ni(II)/Co(II)-sensing RcnR, consistent with factors beyond the primary coordination sphere switching metal selectivity. Competition with chelators mag-fura-2, nitrilotriacetic acid, EDTA, and EGTA estimate K_D Ni(II) for the tightest site of InrS as 2.05 (±1.5) × 10^{-14} M, and weaker K_D Ni(II) for the cells' metal sensors of other types: Zn(II) co-repressor Zur, Co(II) activator CoaR, and Zn(II) derepressor ZiaR. Ni(II) transfer to InrS occurs upon addition to Ni(II) forms of each other sensor. InrS binds Ni(II) sufficiently tightly to derepress Ni(II) export at concentrations below K_D Ni(II) of the other sensors.

The photosynthetic machinery generates special demands for metals in cyanobacteria such as *Synechocystis* PCC 6803 (hereafter referred to as *Synechocystis*): manganese for the oxygen evolving water-splitting enzyme, 22 atoms of iron/pair of photosystems (1), copper for plastocyanin, zinc in carbonic anhydrase to liberate CO_2 for fixation in carboxysomes (2), as examples, and cobalt is needed for cyanocobalamin (whereas higher plants contain no B_{12}-requiring enzymes) (3). Nickel is used by the bidirectional hydrogenase which can generate dihydrogen gas to remove surplus reducing potential from the light reactions of photosynthesis (4). The prospect of engineering cyanobacteria to transduce light into useable bioenergy, for example dihydrogen, has attracted attention (5). The optimization of cofactor supply for critical metalloenzymes may become important for such efforts (6, 7). There is interest in discovering and understanding the action of metal sensors from these bacteria because they modulate metal availability for metalloenzymes.

The *Synechocystis* genome encodes one deduced, but unstudied, representative of the CsoR/RcnR family of DNA-binding metal-responsive transcriptional regulators. CsoR and RcnR sense Cu(I), or Ni(II) and Co(II), in *Mycobacterium tuberculosis* and *Escherichia coli*, respectively (8–10). CsoR-like Cu(I) sensors have also been described in *Bacillus subtilis* (11, 12), *Listeria monocytogenes* (13), *Thermus thermophilus* (14), and *Staphylococcus aureus* (15, 16), plus a second CsoR-like Cu(I) sensor (RicR) has been discovered in *M. tuberculosis* (17). *S. aureus* also contains a paralogue of CsoR, CstR, but this regulates inorganic sulfur metabolism in response to oxidation of its Cys residues by an intermediate in assimilatory sulfate reduction (15). One additional RcnR-like Ni(II) sensor has been characterized (NcrB) from *Leptospirillum ferriphilum* (18). Effort has been directed toward understanding the molecular mechanisms of metal selectivity of CsoR, RcnR, and indeed other types of DNA-binding metal-responsive transcriptional regulators. CsoR has a trigonal Cu(I) site composed of two Cys (residues XZ below) and one His (residue Y below) whereas a combination of x-ray absorption spectroscopy and mutagenesis indicates the presence of a pseudo-octahedral Ni(II) or Co(II) site in RcnR which includes the N-terminal plus one defined Cys and two (or three for Co(II)) deduced His (including residue W below) (8, 10). The allosteric mechanism of CsoR also relies on a Tyr residue (residue A below) which in Cu(I)-CsoR forms a hydrogen bond with the noncoordinating imidazole nitrogen of a Cu(I)-binding His plus a second coordination sphere Glu (residue B below) (8, 19). Together, these

* This work was supported by Biotechnology and Biological Research Council Grants BB/H006052/2 and BB/E001688/1.
⌘ *Author's Choice*—Final version full access.
[S] This article contains supplemental Figs. S1–S14, Table S1, Methods, and additional references.
[1] To whom correspondence should be addressed. E-mail: nigel.robinson@durham.ac.uk.

residues define the WXYZ(AB) motif of CsoR/RcnR sensors (10, 20) (supplemental Fig. S1).

Cytosolic sensors of Ni(II) or of Cu(I) have not been described in *Synechocystis*. The carrier that shuttles electrons between the two photosystems within the thylakoid lumen undergoes a copper-dependent switch. When copper is limiting, heme iron is used in cytochrome c_6, but this is replaced by copper in plastocyanin under copper sufficiency, and the switch occurs at the transcriptional level (21). Such a switch was first described in *Chlamydomonas reinhardtii* (22, 23) where it is controlled by Crr1 (24). The functionally equivalent cyanobacterial Cu(I) sensor remains to be discovered. Expression of the *pacS* gene encoding a Cu(I)-transporting P_1-type ATPase that supplies copper to plastocyanin is also Cu(I)-regulated, but again the Cu(I) sensor remains to be discovered. The periplasmic Ni(II) sensor NrsS modulates the *nrsBACD* Ni(II) efflux operon via the DNA-binding transcriptional regulator NrsR (25, 26), but there is no known cytosolic Ni(II) sensor in *Synechocystis*. Moreover, when the Ni(II)/Co(II) sensor NmtR from *M. tuberculosis* was introduced into a related cyanobacterium, *Synechococcus* PCC 7942, Co(II) sensing was retained, but Ni(II) sensing was lost, suggesting that the buffered concentration of Ni(II) in the cyanobacterial cytosol may be maintained at a lower level than in *M. tuberculosis*, too low for NmtR to gain access to Ni(II) in the heterologous host (27). Supplementation of growth medium with additional Ni(II) increases hydrogenase activity (which can either consume or generate dihydrogen depending upon the enzyme type and environmental conditions) in a range of cyanobacteria (28–32), which is again consistent with a low and limiting buffered concentration of Ni(II) in the cyanobacterial cytosol, but the Ni(II) sensor that maintains this concentration was not known previously.

Known cytosolic metal sensors in *Synechocystis* include cobalt-dependent activator of expression of cobalt efflux, CoaR (33), zinc-dependent derepressor of expression of zinc efflux, ZiaR (34), and zinc-dependent co-repressor of expression of zinc influx, Zur (35, 36). The primary and secondary metal coordination spheres of these sensors must somehow confer different metal selectivities. One untested hypothesis is that selectivity is partly a function of the relative metal affinities of the complement of metal sensors in a cell, regardless of their protein families (6). In this work we characterize the CsoR/RcnR sensor of *Synechocystis*, herein referred to as InrS (internal nickel-responsive sensor) and compare its nickel affinity with cytosolic sensors of other metals including one sensor from each family represented in the *Synechocystis* genome.

EXPERIMENTAL PROCEDURES

Protein Expression Plasmids—sll0176 (Cyanobase annotation) was amplified from *Synechocystis* genomic DNA using primers 1 and 2 (supplemental Table S1) and the resulting fragment cloned (NdeI and BamHI) into pET29a (Novagen) to create pETInrS. pETCoaR was produced in an analogous manner using primers 3 and 4 (supplemental Table S1) to amplify *sll0794* and the resulting fragment cloned (NdeI and EcoRV) into pET29a. The production of pETZiaR (37) and pETZur (36) has been described previously.

Protein Expression and Purification—E. coli strain BL21(DE3) was transformed to kanamycin resistance with pETInrS. Exponentially growing cells were induced with 1 mM isopropyl 1-thio-β-D-galactopyranoside and cultured for a further 2 h before harvest. InrS was purified from soluble cell lysate (postsonication) using nickel affinity, size exclusion, and heparin affinity chromatography (for details, see supplemental Methods). InrS was confirmed to be ≥95% pure by SDS-PAGE, its identity verified by MALDI-peptide mass fingerprinting (Pinnacle, Newcastle University), and mass determined by electrospray ionization-MS (Waters QTD).

CoaR was expressed in 10 × 1-liter cultures of BL21(DE3)pETCoaR induced with 0.2 mM isopropyl 1-thio-β-D-galactopyranoside for 3 h, then recovered from the insoluble cell lysate by the inclusion of 0.8% w/v *n*-dodecyl β-D-maltoside in the buffer. CoaR was then further purified by nickel affinity, cation exchange, and heparin affinity chromatography (see supplemental Methods). Purity (>90%) was tested by SDS-PAGE. Expression and purification of ZiaR (37) and Zur (36) have been described previously; masses were determined by electrospray ionization-MS.

Anaerobic protein stocks were produced as described previously (37) (with 0.1% w/v *n*-dodecyl β-D-maltoside included in CoaR buffers). CoaR, ZiaR, and Zur concentrations were estimated by measurement of $A_{280\ nm}$ and via theoretical extinction coefficients, 26,930 $M^{-1}\ cm^{-1}$, 5,960 $M^{-1}\ cm^{-1}$, and 7,450 $M^{-1}\ cm^{-1}$, respectively. To quantify InrS (which has no fluorescent residues), Bradford assays were calibrated against BSA using a conversion factor (1.2) estimated from sequence composition and also validated by quantitative amino acid analysis (see supplemental Methods). Cys residues in InrS, ZiaR, and Zur were >95% reduced as determined with 5,5′-dithiobis-(2-nitrobenzoic acid) (DTNB) (38, 39). CoaR gave less consistent reactivity of all thiols with DTNB although DNA binding or metal binding did not vary. All proteins were verified to be >95% apo by ICP-MS.[2]

UV-Visible Absorption Spectroscopy—Spectra were recorded under anaerobic conditions on either a Perkin Elmer λ35 or Cary 4E UV-visible spectrophotometer. InrS was diluted in Chelex-treated and N_2-purged 10 mM HEPES, pH 7.8, 100 mM NaCl, 400 mM KCl in gas-tight quartz cuvettes (Hellma). Metal additions (CuCl, $NiSO_4$, $CoCl_2$) were made either in an anaerobic glove box (Belle Technology) mixing by aspiration or from a gas-tight syringe mixing by inversion. [Ni(II)] and [Co(II)] stocks were verified by ICP-MS. Cu(I) was prepared as described previously (37). Spectra were recorded at 5-min intervals to equilibrium.

Construction of ΔinrS Deletion Strain—Primers 5 and 6 (supplemental Table S1) were used to amplify a 4.2-kb fragment containing *sll0176* and flanking regions from genomic DNA and product ligated to pGEM-T (Promega). Primers 7 and 8 (supplemental Table S1) were used to remove the NdeI restriction site from the pGEM-T multicloning site via QuikChange

[2] The abbreviations used are: ICP-MS, inductively coupled plasma mass spectrometry; CAT, chloramphenicol acetyltransferase; LMCT, ligand to metal charge transfer; mf2, mag-fura-2; NTA, nitrilotriacetic acid; RLM-RACE, RNA ligase-mediated rapid amplification of complementary ends.

mutagenesis (Stratagene). Primers 9 and 10 followed by 11 and 12 (supplemental Table S1) were used to introduce NdeI restriction sites toward both ends of *sll0176*. Following excision of the bulk of *sll0176* from the plasmid using NdeI the chloramphenicol acetyltransferase gene (CAT) was ligated in its place to create pGEM*sll0176*::CAT. SacII and PstI were used to excise the CAT cassette disrupted *sll0176* fragment which was incubated with *Synechocystis* to transform the cells to chloramphenicol resistance. Transformants were selected on BG11 plates (40 μg ml^{-1} chloramphenicol) prior to growth in BG11 (7.5 μg ml^{-1} chloramphenicol). Deletion of *inrS* by insertion of the CAT cassette and segregation to all chromosomal copies were confirmed by PCR using primers 13 and 14 (supplemental Table S1) to identify a diagnostic 4.9-kb fragment (wild type (WT) gives a 4.3-kb fragment).

Isolation of RNA and Reverse Transcription PCR—Logarithmically growing cells were inoculated to $A_{600\ nm} = 0.1$ in standard BG11 or BG11 supplemented with maximum noninhibitory concentrations of $NiSO_4$ (0.5 μM), $ZnSO_4$ (12 μM), $CoCl_2$ (2.0 μM), or $CuSO_4$ (1.0 μM) (concentrations confirmed in a series of growth yield experiments to give <10% inhibition) and cultured for 48 h. Total RNA was extracted as described previously (40), and following DNaseI treatment, cDNA was produced using an ImPromII kit (Promega). Reverse transcriptase was omitted from negative controls. Transcript abundance was assessed by PCR with primers 15 and 16 (*nrsD*), 17 and 18 (*nrsB*), 19 and 20 (*rps1*, control) (supplemental Table S1) designed to amplify ~300 bp of each.

Electrophoretic Mobility Shift Assay—The entire *nrsC-nrsD* intergenic region was amplified from genomic DNA using primers 21 and 22 (supplemental Table S1) then ligated to pGEM-T to create pGEM*nrsD*Pro. The specific *nrsD*Pro DNA fragment was amplified from pGEM*nrsD*Pro using primers 21 and 22 (supplemental Table S1). The nonspecific DNA fragment (ns DNA), consisting of sequence from the pGEM-T multicloning site and flanking regions, was amplified from recircularized empty pGEM-T using primers 23 and 24 (supplemental Table S1). InrS was incubated for 30 min at room temperature with *nrsD*Pro and ns DNA (100 nM each) with varying [InrS] in 10 mM HEPES, pH 7.8, 300 mM NaCl, 2 mM DTT, 2 mM EDTA, 3% glycerol (v/v), and 0.05 mM spermidine, then resolved by native PAGE (TBE buffer system) (41), bands visualized with ethidium bromide.

Fluorescence Anisotropy—Complementary, fluorescently labeled oligonucleotides 25 and 26 (supplemental Table S1) (which contain the InrS DNA binding site predicted by bioinformatics and tested by electrophoretic mobility shift assays) were annealed by heating a 10 μM concentration of each strand in 10 mM HEPES, pH 7.8, 150 mM NaCl to 95 °C then cooling overnight (*nrsD*ProFA). InrS was prepared in 10 mM HEPES, pH 7.8, 200 mM NaCl, 800 mM KCl (Chelex-treated) and 1 mM DTT, with or without 5 mM EDTA or $NiSO_4$ (1.2 molar eq relative to [InrS]). *nrsD*ProFA (10 nM) was incubated in 10 mM HEPES, pH 7.8, 60 mM NaCl, 240 mM KCl (Chelex-treated) and 1 mM DTT, with or without 5 mM EDTA (25 °C, 20 min) before titration with InrS, Ni(II)-InrS, or InrS followed by $NiSO_4$. Changes in anisotropy were measured using a modified Cary Eclipse Fluorescence Spectrophotometer (Agilent Technologies) fitted with polarizing filters ($\lambda_{ex} = 530$ nm, $\lambda_{em} = 570$ nm, averaging time = 20 s, replicates = 5).

RNA Ligase-mediated Rapid Amplification of 5′-Complementary Ends—5′-RLM-RACE was performed using the FirstChoice RLM-RACE kit (Applied Biosystems) according to the manufacturer's instructions with RNA extracted from cells grown in BG11 with and without Ni(II) or Co(II) supplemented to maximum noninhibitory concentrations, as described above. *nrsD* transcripts were amplified by nested PCR using primers 27 and 28 (supplemental Table S1) along with primers included in the kit (specific to the 5′-adapter). Fragments were cloned in pGEM-T for sequencing.

Phenotypic Assays—Strains (WT and Δ*inrS*) were inoculated to $OD_{800\ nm} = 0.075$ and cultured with or without 0.5 μM $NiSO_4$ for 24 h. Cell numbers were recorded using a Casy Cell Counter TT (Innovatis) before harvesting 20 ml of each culture at 3,900 × *g*. Cell pellets were washed with 50 mM Tris, pH 7.5, 0.5 M sorbitol, and 100 μM EDTA (3 × 10 ml) then suspended in ultrapure 65% v/v HNO_3 (1 ml) and left to digest prior to metal analysis by ICP-MS. Visible absorption spectra of logarithmically growing cells inoculated to $OD_{800\ nm}$ ~0.3 were recorded using a Multiskan GO microplate reader and spectrophotometer (Thermo Scientific). Fluorescence emission spectra were recorded using a Cary Eclipse Fluorescence Spectrophotometer (Varian) ($\lambda_{ex} = 442$ nm, $\lambda_{em} = 500 - 800$ nm). Pigments were extracted from pelleted WT and Δ*inrS* cells (equivalent to a total $OD_{800\ nm} = 10$ in 1 ml) in mid-logarithmic growth. Cells were suspended in 100 μl of BG11 before addition of 2 ml of *N,N*-dimethylformamide, vortexed for 1 min, centrifuged at 3,900 × *g*, and the absorption spectrum of the supernatant was used to quantify chlorophyll *a* and carotenoids with established formulas (42) [Carotenoids] (μg ml^{-1}) = ($A_{461\ nm} - 0.046 \times OD_{664\ nm}$) × 4, [Chl *a*] ($\mu$g ml^{-1}) = $1.21 \times OD_{664\ nm} - 0.17 \times A_{625\ nm}$.

Protein Chelator-Nickel Competition—Experiments were carried out in Chelex-treated and N_2-purged 10 mM HEPES, pH 7.8, 100 mM NaCl, 400 mM KCl under anaerobic conditions. Chelators (NTA, EGTA, and EDTA) were incubated with Ni(II) for 10 min before adding InrS. $A_{333\ nm}$ was monitored every 30 s (Perkin Elmer λ35 spectrophotometer) to equilibrium and used in conjunction with calibration curves produced by titration of InrS with Ni(II) to calculate affinity constants (detailed in supplemental Fig. S8). The nickel affinities of ZiaR, Zur, and CoaR were determined by competition with the fluorescent chelator mf2 (quantified via $\epsilon = 22{,}000$ M^{-1} cm^{-1} at 369 nm) (43) and NTA for CoaR. mf2 was incubated with Ni(II) for 10 min before adding protein. Fluorescence emission of mf2 was monitored every 30 s ($\lambda_{ex} = 380$ nm, $\lambda_{em} = 505$ nm) to equilibrium, and affinity constants were calculated in conjunction with a concurrently produced standard curve of mf2 fluorescence emission upon titration with Ni(II) (for details, see supplemental Fig. S8). Ni(II) or Ni(II)-NTA was added to CoaR and intrinsic fluorescence emission of CoaR recorded ($\lambda_{ex} = 280$ nm, $\lambda_{em} = 300 - 400$ nm).

Interprotein Nickel Exchange—Proteins (ZiaR, Zur, and CoaR) were preincubated with Ni(II) in 10 mM HEPES, pH 7.8, 100 mM NaCl, 400 mM KCl for Zur, with 0.1% w/v *n*-dodecyl β-D-maltoside (Chelex-treated) for CoaR, and 10 mM HEPES,

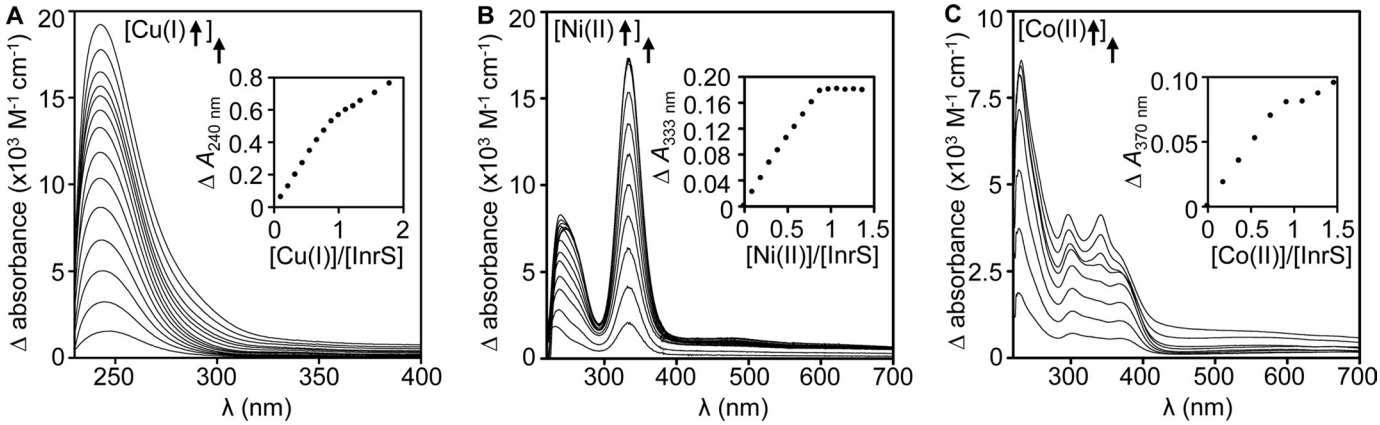

FIGURE 1. **Cu(I), Ni(II), and Co(II) bind to InrS with spectral features more similar to CsoR than RcnR.** Apo-subtracted UV-visible difference spectra of InrS titrated with *A*, Cu(I), *B*. Ni(II) and *C*, Co(II) using 40, 10.4, and 32.7 μM InrS, respectively (data expressed per mole InrS monomer l^{-1} cm^{-1}), are shown. *Insets* are binding isotherms at selected absorbance maxima.

pH 7.8, 40 mM NaCl, 160 mM KCl for ZiaR (under anaerobic conditions). InrS was added and equilibria assessed. For the competition between Zur and InrS the quenching of intrinsic fluorescence of Zur by Ni(II) was monitored (fluorometer settings as for CoaR/NTA Ni(II) competition, above). For the competition between ZiaR and InrS the mixture was applied to a 1-ml heparin column (GE Healthcare) and eluted over 6 × 0.5-ml fractions with buffer containing 10 mM HEPES, pH 7.8, [NaCl:KCl, 1:4] = 0.5 M followed by 6 × 0.5-ml fractions with the above buffer with [NaCl:KCl, 1:4] = 1 M. Nickel was assayed by ICP-MS and protein by SDS-PAGE. For the competition between CoaR and InrS the change in Ni(II)-dependent spectral features upon addition of InrS was monitored.

RESULTS

InrS Binds Cu(I) or One Equivalent of Ni(II) with UV-Visible Difference Spectra Similar to CsoR—The metal binding properties of InrS were analyzed with a view to identifying candidate metal effectors. Recombinant InrS (molecular mass 11,887 consistent with cleavage of the N-terminal Met) migrates with an apparent molecular mass >44 kDa by native size exclusion chromatography, indicative of a tetramer (supplemental Fig. S2). Addition of Cu(I) to an anaerobic solution of InrS generates metal-dependent spectral features of absorbance at 240 nm ≈ 14,000 M^{-1} cm^{-1} for a 1:1 Cu(I)-InrS complex, expressed per mol of InrS monomer/liter per cm (Fig. 1*A*). The spectrum does not saturate at 1 eq of Cu(I) (Fig. 1*A inset*) but is otherwise similar to that of Cu(I)-CsoR from several bacteria (8, 12, 15). Ni(II)-InrS shows an intense feature at 333 nm ($\epsilon_{333\ nm}$ ≈ 17,200 M^{-1} cm^{-1}, Fig. 1*B*) reminiscent of Ni(II)-CsoR (*B. subtilis*) ($\epsilon_{340\ nm}$ ≈ 11,500 M^{-1} cm^{-1}) (12), assigned as ligand to metal charge transfers (LMCT) due to nickel-thiolate bonds. The feature at 333 nm saturates at 1 eq of Ni(II) (Fig. 1*B*, *inset*), and a ~1:1 Ni(II)-InrS complex co-migrates in size exclusion chromatography (supplemental Fig. S3). The Ni(II) coordination environment of RcnR is distinct from InrS with features below 300 nm and not between 330 and 340 nm (10). Co(II)-InrS LMCTs differ from RcnR and CsoR with multiple features between 290 nm and 400 nm (Fig. 1*C* and supplemental Fig. S4). The intensities of Co(II)-dependent LMCTs in the 290 to 400 nm region (within the range of 2,000–3,000 M^{-1} cm^{-1}) are indicative of two Co(II)-thiolate bonds/monomer ($\epsilon_{318\ nm}$ in the range 900–1,200 M^{-1} cm^{-1} reporting on each Co(II)-thiolate bond in other proteins) (44), and recombinant InrS contains two Cys. The *d-d* transition envelope centered at 600 nm ($\epsilon \approx 200\ M^{-1}\ cm^{-1}$ using a sample incubated with 1 eq of Co(II) (supplemental Fig. S4)) is sufficiently intense to suggest a tetrahedral Co(II)-InrS complex, similar to Co(II)-CsoR but unlike Co(II)-RcnR (10, 12). The Co(II)-dependent spectral features saturate between 1.5 and 2 eq (supplemental Fig. S4). Ni(II)-InrS exhibits *d-d* transitions at $\lambda_{max} \approx 480$ nm (supplemental Fig. S4) consistent with Ni(II) coordinated in a square planar or distorted square planar environment but too intense for an octahedral environment (12, 45).

InrS Represses Final Open Reading Frame in nrs Operon—The spectral properties of InrS-metal complexes are more similar to CsoR than RcnR, and the ability to form InrS-DNA complexes was therefore tested with (i) the upstream regions of known copper-responsive genes *pacS* and *petE* (plastocyanin) and (ii) upstream gene regions that contain nucleotide sequences with some similarity to the *B. subtilis* CsoR DNA binding site and additionally with connection to copper (*moeA*, involved in copper to molybdenum substitution in molybdopterin biosynthesis, and *coxB*, cytochrome *c* oxidase subunit II). No specific retardation was detected in assays with upstream regions of *pacS* or *petE*, but some specific binding, with an apparent DNA binding affinity K_{DNA} weaker than 8 μM, was detected with *moeA* and *coxB* giving solely large InrS-DNA complexes (supplemental Fig. S5).

During the course of this work a consensus nucleotide binding sequence was reported for CsoR-like proteins (15) (Fig. 2*A*), and this was used to search regions (300 bp) upstream of *Synechocystis* ORFs. The best match also has a diagnostic (of CsoR/RcnR DNA binding sites) CG-rich sequence (46) but lies within the *nrs* polycistronic transcript (25) (Fig. 2*A*). Because the deduced binding site is upstream of *nrsD*, whose product is predicted to export Ni(II) across the plasma membrane, this raised the intriguing possibility that a cytosolic metal sensor might additionally regulate the final gene in the *nrs* operon independently via a cryptic promoter in the *nrsC-nrsD* intergenic region (Fig. 2*A*).

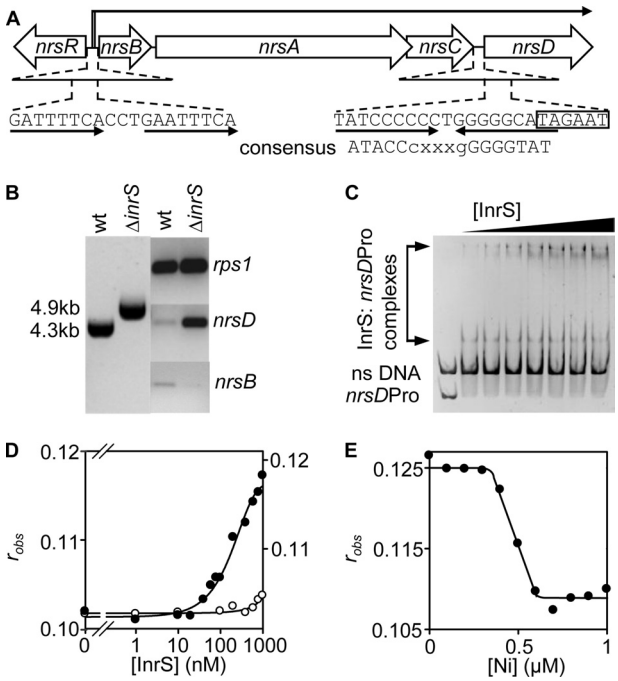

FIGURE 2. **InrS binds upstream and represses expression of *nrsD* within the *nrs* Ni(II) efflux operon.** *A*, representation of the *nrs* operon (to scale). The deduced NrsR binding site between *nrsR* and *nrsB* (26) and consensus CsoR/CstR inverted repeat (15) located between *nrsC* and *nrsD*, are shown along with an overlapping Pribnow box (*boxed*). Known transcriptional start sites of the *nrsBACD* transcript (26) are also shown. *B*, *left*, PCR amplification of *inrS* flanking regions from WT and Δ*inrS* cells confirming integration and segregation to all chromosomes in Δ*inrS*. *Right*, RT-PCR analysis of *nrsD*, *nrsB* and *rps1* transcript abundance in WT and Δ*inrS*. *C*, specific retardation of the *nrsC-nrsD* intergenic region by InrS shown by mobility shift assay. *nrsD*Pro and ns DNA were incubated with 0, 8, 12, 16, 20, 24, 28, and 32 μM InrS (analogous to [InrS] in supplemental Fig. S5). *D*, titration of *nrsD*ProFA, with apo-InrS (*filled circles*) (*left* axis) or Ni(II)-InrS (*open circles*) (*right* axis). *E*, titration of preformed apo-InrS-*nrsD*ProFA complexes with $NiSO_4$ (using 1 μM Inrs).

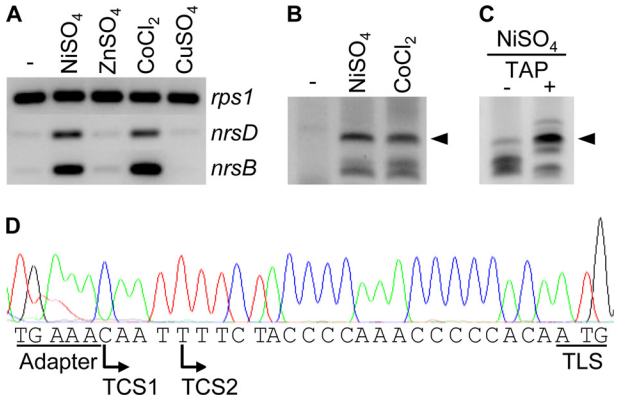

FIGURE 3. **RLM-RACE identifies Ni(II)- and Co(II)-responsive transcription start sites in the *nrsC-nrsD* intergenic region.** *A*, RT-PCR analysis of *nrsD*, *nrsB*, and *rps1* transcript abundance in WT and Δ*inrS* in response to maximum noninhibitory concentrations of four metal salts. *B*, RLM-RACE using RNA from WT cells exposed to maximum noninhibitory concentrations of $NiSO_4$ and $CoCl_2$. *C*, separate RLM-RACE experiment with RNA extracted from Ni(II)-treated cells in which tobacco acid pyrophosphatase treatment was omitted from the control sample. The indicated products are of the expected size (~400 bp) for transcripts originating from an *nrsD* promoter. The abundance of the ~400 bp PCR products increase in a tobacco acid pyrophosphatase (*TAP*)-dependent manner. *D*, the ~400-bp products were cloned, sequenced, and the 3′ end of the adapter is indicated along with transcriptional start site (*TCS1*) and the translational start site (*TLS*). A separate RLM-RACE experiment identified an alternate transcriptional start site (TCS2) 4 bp downstream of TCS1.

A mutant deficient in InrS was generated by homologous recombination-mediated insertion of the CAT gene within ORF *sll0176* (*inrS*). Insertion and segregation were confirmed via PCR with genomic DNA recovered from the mutant demonstrating loss of all WT *sll0176* product (~4.3 kb) and appearance of a larger fragment (~4.9 kb) diagnostic of CAT gene insertion, and the strain was designated Δ*inrS* (Fig. 2*B*). Increased abundance of *nrsD*, but crucially not *nrsB*, transcripts were detected in total RNA from Δ*inrS* relative to WT by RT-PCR (Fig. 2*B*). Although there was not an equivalent increase in abundance of *coxB* or *moeA* transcripts in the mutant, *moeA* transcripts did show some elevation in Δ*inrS* cells, but *moeA* was not responsive to exogenous nickel or copper (supplemental Fig. S6). Taken together, data presented here imply the *pacS*, *petE*, *moeA*, and *coxB* promoters are not targets for metalloregulation by InrS.

InrS specifically retards a DNA fragment containing part of the *nrsC-nrsD* intergenic region generating low molecular mass complexes in addition to high molecular mass complexes (Fig. 2*C*). Binding to this DNA fragment is tighter than to other fragments tested in supplemental Fig. S5. The effects of Ni(II) on DNA binding were examined under equilibrium conditions by fluorescence anisotropy (Fig. 2, *D* and *E*). Titration of hexachlorofluorescein-labeled 33-bp *nrsD* operator-promoter (*nrsD*-ProFA) with apo-InrS showed an increase in anisotropy reporting on the formation of InrS-DNA complexes with apparent K_{DNA} ~ 100 nM (Fig. 2*D*). Crucially, the apparent K_{DNA} is at least 1 order of magnitude weaker for Ni(II)-InrS than for apo-InrS (Fig. 2*D*); moreover, addition of Ni(II) to preformed InrS-DNA complexes leads to loss of DNA binding (Fig. 2*E*). Thus, InrS represses expression of the last gene in the *nrs* operon (*nrsD*) and binds specifically to a hypothetical *nrsD* operator-promoter as an inverse function of [Ni(II)].

Identification of Ni(II)-regulated Transcription Start Sites between nrsC and nrsD—The possibility that expression of *nrsD* is also driven in response to metal from a cryptic promoter in the *nrsC-nrsD* intergenic region was examined. RT-PCR confirmed an accumulation of *nrsD* transcripts in response to maximum noninhibitory concentrations of nickel and cobalt, but not copper or zinc salts (Fig. 3*A*). It is possible that these transcripts could be solely products of expression from the two-component NrsS-NrsR-regulated *nrs* promoter, and indeed *nrsB* transcripts accumulate in response to the same two metals (Fig. 3*A*), as reported previously (25). However, nickel- and cobalt-responsive short *nrsD* products of a diagnostic size (~400 bp) for initiation within the *nrsC-nrsD* intergenic region were identified by 5′-RLM-RACE (Fig. 3*B*). Short products of other sizes were detected with varying relative abundance in replicate experiments, but only the ~400-bp product was dependent upon tobacco acid pyrophosphatase treatment, diagnostic of a triphosphate-capped mRNA as opposed to degraded mRNA (Fig. 3*C*). Cloning and sequence analysis of the ~400-bp products revealed two transcription start sites upstream of the *nrsD* initiation codon (Fig. 3*D*), 10 and 14 bp downstream of the mid-point of a candidate Pribnow box (5′-TAGAAT-3′), which overlaps the deduced InrS binding site (Fig. 2*A*).

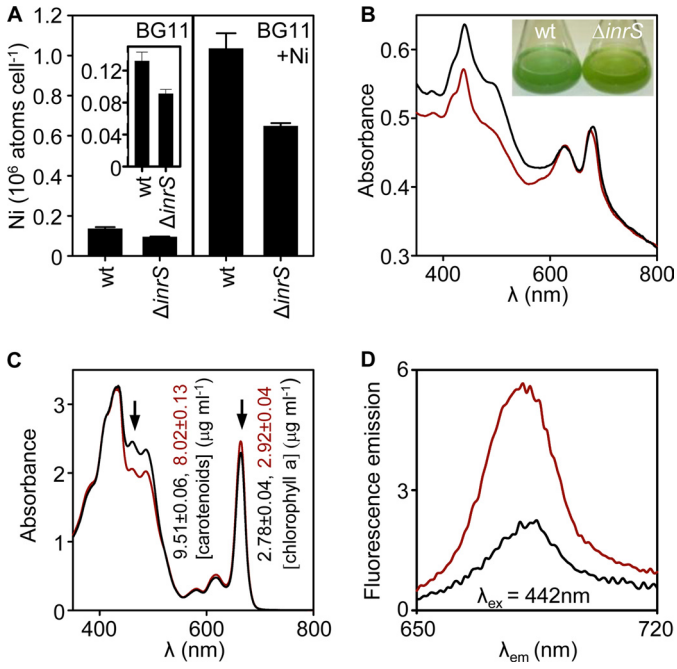

FIGURE 4. **Nickel-homeostasis and pigments are altered in Δ*inrS* mutants.** *A*, whole cell nickel content of WT and Δ*inrS* cells cultured in standard media (*left* and *inset*) or exposed to maximum noninhibitory [Ni(II)] (*right*). *B*, absorption spectra of WT (*red*) and Δ*inrS* (*black*) cells normalized to $OD_{800\ nm}$ ~0.3. *Inset*, cultures of both genotypes. *C*, absorption spectra of *N,N*-dimethylformamide-extracted pigments from WT (*red*) and Δ*inrS* (*black*) cells with mean concentration (± S.D.) of carotenoids derived from absorbance at 461 nm and chlorophyll *a* derived from absorbance at 664 nm for WT (*red*) and Δ*inrS* (*black*). *Arrows* indicate wavelengths used to calculate concentrations of carotenoids (461 nm) and chlorophyll *a* (664 nm). *D*, chlorophyll *a* fluorescence emission of cultures used in *B*.

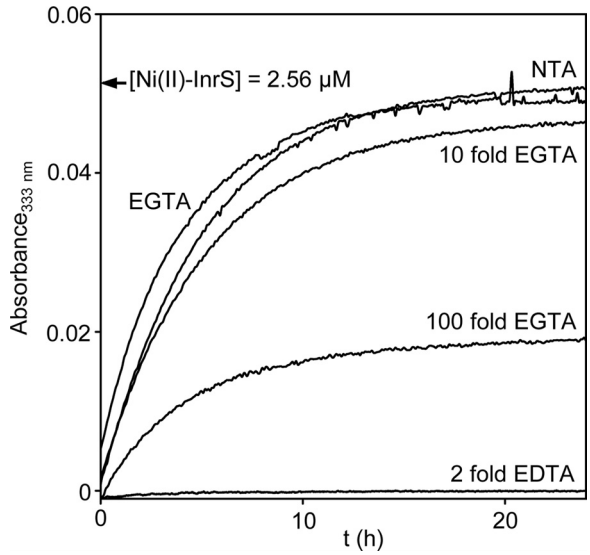

FIGURE 5. **Ni(II) affinity of InrS.** InrS (10.3–10.4 μM) was added to a solution of NTA (10 μM) or EGTA (10, 100, or 1000 μM) preincubated with Ni(II) (2.56 μM). Exchange of Ni(II) to InrS was monitored by $A_{333\ nm}$ (every 30 s, data shown is a sampling of every tenth data point) which reports on Ni(II)-InrS formation (Fig. 1*B*). The absorbance of 2.56 μM Ni(II)-InrS calculated from Fig. 1*B inset* is shown to indicate the maximum absorbance expected after full transfer of Ni(II) to InrS. Competition with EDTA was carried out in a analogous manner ([InrS] = 24.2 μM, [EDTA] = 50 μM, [Ni(II)] = 25 μM).

*Ni(II)-related Phenotypes of Δ*inrS* Cells*—The connection between InrS and Ni(II) homeostasis was further supported by assays of metal content of the deletion mutant. Cells missing InrS are expected to show constitutive Ni(II) export to the periplasm, and this is consistent with a reduction in Ni(II) content from 1.0 to 0.64 million atoms $cell^{-1}$ when grown in medium supplemented with the maximum noninhibitory [nickel] for WT and 0.13–0.091 million atoms $cell^{-1}$ in standard medium (Fig. 4*A*). In contrast, the copper content of Δ*inrS* shows negligible change (supplemental Fig. S7). There was a slight, but reproducible, increase in nickel tolerance in Δ*inrS* (supplemental Fig. S7).

Cultures of Δ*inrS* could be discerned from other strains due to a subtle change in pigmentation (Fig. 4*B*, *inset*), subsequently defined as an increase in absorption below 600 nm (Fig. 4*B*). The levels of phycocyanin (A_{max} = 630 nm) and chlorophyll *a* (OD_{max} = 680 nm; note A_{max} = 664 nm in solvent extracted pigments) appear normal, yet absorption in the region of 442 nm (the second maxima for chlorophyll *a*) is elevated in Δ*inrS*, suggestive of an increased abundance of other pigments that co-absorb at this wavelength (47). Quantification of solvent-extracted pigments confirms an increase in carotenoids in Δ*inrS* (Fig. 4*C*). Most importantly, fluorescence emission from chlorophyll *a* is greatly reduced in Δ*inrS* excited at 442 nm (Fig. 4*D*), consistent with the effects of protective pigments, such as carotenoids (48, 49), reducing the demand for Ni(II)-requiring hydrogenase activity.

InrS Outcompetes NTA and EGTA but Not EDTA for Ni(II)—To explore metal selectivity, the affinity of InrS for Ni(II) at the tightest site (per tetramer) was determined. Apo-InrS was added to a Ni(II)-NTA mix (using equimolar InrS and NTA), and the formation of Ni(II)-InrS was monitored via absorbance at 333 nm, establishing that at equilibrium Ni(II) fully partitions to InrS (Fig. 5). In a similar experiment with equimolar EGTA, again Ni(II) partitions to InrS whereas in contrast a 2-fold molar excess of EDTA fully outcompetes InrS, placing the Ni(II) affinity of InrS in a range between these chelators (the EGTA-Ni(II), and EDTA-Ni(II) affinity constants corrected for pH using Schwarzenbach's α-coefficient method (see supplemental Methods), are K_D 1.36×10^{-11} M and 1.00×10^{-16} M, respectively). At 10-fold and 100-fold excess of EGTA Ni(II) partitions between InrS and chelator (Fig. 5). The equilibrium concentration of Ni(II)-InrS calculated from the end points on Fig. 5 using the calibration curve on Fig. 1*B*, *inset*, or supplemental Fig. S8, estimate K_D InrS for Ni(II) of 8.30×10^{-15} M (10-fold excess of EGTA) and 3.67×10^{-14} M (100-fold excess of EGTA). The experiment was further replicated to generate a mean K_D Ni(II) InrS of 2.05 (± 1.5) $\times 10^{-14}$ M (supplemental Fig. S8).

Synechocystis Sensors of Other Metals from Other Families Bind Ni(II) More Weakly—What are the relative (to 2×10^{-14} M) Ni(II) affinities of the tightest exchangeable binding site of sensors that detect other metals in the cytosol of *Synechocystis*? In addition to InrS, *Synechocystis* contains genes encoding deduced proteins with sequence similarity to four other families of metal sensors, MerR-like (*e.g.* CoaR) (33), Fur-like (*e.g.* Zur) (35, 36), ArsR-SmtB-like (*e.g.* ZiaR) (34,) and CopY-like (50), however the deduced CopY homologue (Slr0240) is conspicuously truncated and missing candidate C-terminal metal-sensing residues (51) (Fig. 6*A*). A sensor from each family has been expressed and purified (Fig. 6, *B–D*), and the affinity for Ni(II) was determined. Incubation of ~equimolar ZiaR with the

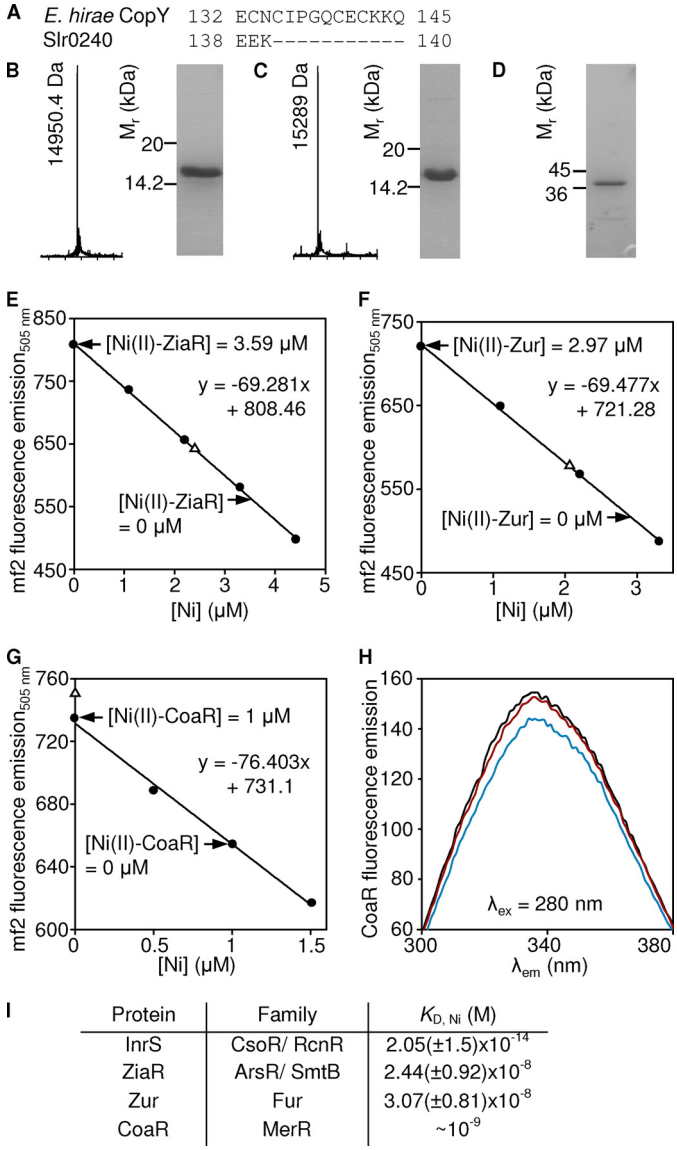

I

Protein	Family	$K_{D,\,Ni}$ (M)
InrS	CsoR/ RcnR	$2.05(\pm1.5)\times10^{-14}$
ZiaR	ArsR/ SmtB	$2.44(\pm0.92)\times10^{-8}$
Zur	Fur	$3.07(\pm0.81)\times10^{-8}$
CoaR	MerR	$\sim10^{-9}$

FIGURE 6. **Ni(II) affinities of other metal sensors from *Synechocystis*.** *A*, alignment of the carboxyl region of *Enterococcus hirae* CopY with that of the deduced product of *slr0240*. *B*, electrospray ionization-MS and SDS-PAGE of purified ZiaR. *C*, purified Zur with masses corresponding to proteins without N-terminal Met. *D*, SDS-PAGE of purified CoaR. *E*, competition between ZiaR and mf2 for Ni(II). mf2 (9.64 μM) was titrated with Ni(II) and fluorescence emission recorded (*solid circles*). ZiaR (7.2 μM) was added to a solution of mf2 (9.64 μM) preincubated with Ni(II) (3.59 μM) and mf2 fluorescence emission monitored to equilibrium (*open triangle*). The linear regression was used to calculate the equilibrium [Ni(II)-ZiaR]. *F*, competition between Zur (6.15 μM) and mf2 (8.8 μM) for Ni(II) (2.97 μM). *G*, CoaR (2 μM) and mf2 (9.25 μM) for Ni(II) (1 μM) both analogous to *E*. *H*, fluorescence emission spectra of apo-CoaR (2.5 μM) (*black line*) and CoaR plus NTA (2.5 μM) preincubated with Ni(II) (2 μM) (*red line*). Subsequent Ni(II) addition in excess (2.5 μM) of [NTA] quenches fluorescence (*blue line*) to an extent similar to a single addition of 2.5 μM Ni(II) in the absence of NTA (supplemental Fig. S10). *I*, Ni(II) affinities of Co(II) activator CoaR, Zn(II) co-repressor Zur, Zn(II) derepressor ZiaR plus InrS. Data are the means of triplicate determinations (from above and supplemental Fig. S9 for ZiaR and Zur; from Fig. 5 and supplemental Fig. S8 for InrS) with S.D. (range estimated from above for CoaR).

fluorescent metal chelator mf2 resulted in partial Ni(II) occupancy of sensor and chelator at equilibrium, enabling estimation of K_D Ni(II) of the tightest site (per dimer) as 2.44 ($\pm$ 0.92) $\times$ 10^{-8} M (Fig. 6*E* and supplemental Fig. S9). Analogous experiments with Zur gave K_D Ni(II) of the tightest site (per dimer) as 3.07 ($\pm$ 0.81) $\times$ 10^{-8} M (Fig. 6*F* and supplemental Fig. S9). Even with a ~4-fold excess of chelator, CoaR outcompeted mf2, implying K_D Ni(II) numerically $\leq$ 10^{-9} M (Fig. 6*G*). Conversely, equimolar NTA fully outcompeted CoaR such that quenching of CoaR autofluorescence was only detected after saturation of the Ni(II) sites of NTA, implying K_D Ni(II) numerically $\geq$ 10^{-9} M (Fig. 6*H* and supplemental Fig. S10). Thus, CoaR, in common with the two zinc sensors, binds Ni(II) more weakly than InrS (Fig. 6*I*).

Ni(II) Partitions to InrS from Zur, ZiaR, and CoaR—To confirm that InrS outcompetes each of the other sensors for Ni(II), apo-InrS was added to Ni(II)-bound forms of Zur, ZiaR, and CoaR, and reactions were analyzed for metal exchange. Unlike InrS, Zur has fluorescent residues (five Tyr) allowing the proteins to be distinguished by fluorescence. Addition of Ni(II) to Zur quenches intrinsic InrS fluorescence, and this is reversed upon addition of apo-InrS (Fig. 7*A*). ZiaR also contains fluorescent residues (four Tyr); however, there is no change in fluorescence upon addition of Ni(II) (supplemental Fig. S11). Metal transfer was thus monitored by ICP-MS after separation by heparin affinity chromatography after addition of apo-InrS to Ni(II)-ZiaR. Ni(II) becomes associated with InrS with negligible amounts retained on ZiaR (Fig. 7*B*). Addition of apo-InrS to Ni(II)-CoaR, which exhibits negligible absorbance between 300–400 nm), generates a spectral feature at 333 nm of equivalent intensity to that obtained with identical concentrations of Ni(II)-InrS alone (Fig. 7*C*). Thus, apo-InrS avidly removes Ni(II) from Ni(II) species of the other three sensors.

DISCUSSION

In this research we discover cryptic transcription start sites within the *nrs* operon which enable independent (of other *nrs* genes) transcription of *nrsD* in response to cytosolic Ni(II) (Figs. 2 and 3 and supplemental Figs. S5 and S6). When surplus Ni(II) accumulates in the periplasm the *nrs* operon is expressed under the control of NrsS/NrsR, allowing efflux across the outer membrane (25, 26), but it is now evident that surplus Ni(II) in the cytosol is also sensed by a DNA-binding protein of the CsoR/RcnR family which represses *nrsD*. Ni(II)-dependent derepression of *nrsD* alone will allow export from the cytosol to the periplasm consistent with enhanced nickel resistance and reduced nickel accumulation of Δ*inrS* (Fig. 4 and supplemental Fig. S12). That Ni(II) is the metal effector of this new family member implies analogy to RcnR, yet its metal-dependent spectral properties are more akin to those of Cu(I)-sensing CsoR (Fig. 1), and hence the protein is independently named InrS (for internal nickel-responsive sensor); however, these observations question why InrS responds to Ni(II) rather than Cu(I).

CsoR binds Cu(I) in a trigonal coordination site which includes imidazole Nδ1 of His-61; Cu(I) binding repositions the nonliganding imidazole Nϵ2 to form hydrogen bonds with Tyr-35 and Glu-81 (second shell AB residues) (8). Replacement of His-61 with unnatural analogues unable to form such hydrogen bonds prevents allosteric coupling of Cu(I) binding to DNA binding (19). An AB motif residue is substituted with Pro in InrS (supplemental Fig. S1). Thus, a primary coordination shell similar to Cu(I)-CsoR in Cu(I)-InrS may be ineffective at trans-

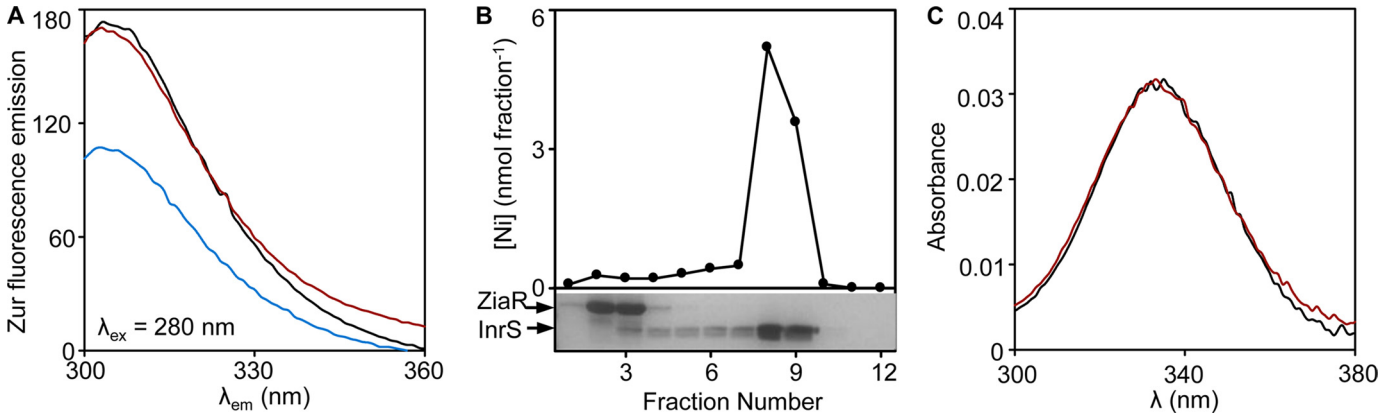

FIGURE 7. **Ni(II) partitions from Zur, ZiaR, and CoaR to InrS.** *A*, fluorescence emission spectrum of apo-Zur (10 μM) (*black line*) and following quenching with Ni(II) (10 μM) (*blue line*). Addition of apo-InrS (10 μM) to Ni(II)-Zur fully alleviates quenching (*red line*). *B*, ZiaR (20 μM) equilibrated with Ni(II) (9.5 μM) before addition of apo-InrS (20 μM). Proteins were separated by heparin affinity chromatography and fractions assayed for nickel by ICP-MS and protein by SDS-PAGE. *C*, absorption spectrum of Ni(II)-InrS (2.4 μM Ni(II), 5 μM InrS) (*black line*). Addition of apo-InrS (5 μM) to Ni(II)-CoaR (2.4 μM Ni(II), 5 μM CoaR, which shows negligible absorbance in this region and is used as base line) generates a spectrum (*red line*) which overlays that for 2.4 μM Ni(II)-InrS.

ducing this signal due to the absence of a vital secondary shell residue.

Clearly, Ni(II) does drive the allosteric mechanism of InrS (Figs. 2 and 3). The spectral feature of Ni(II)-InrS at 333 nm has similarity to Ni(II)-substituted CsoR and to Ni(II)-NikR (12, 45). The *d-d* transition and LMCT features of Ni(II)-InrS are within the range of wavelengths and intensities for model complexes containing at least one sulfur ligand and square planar (but not octahedral) geometry (52); the spectra are also dissimilar to Ni(II)-substituted proteins with tetrahedral geometry (53, 54). Additionally, in contrast to Co(II)-RcnR the extinction coefficient for *d-d* transitions observed in Co(II)-InrS suggests the presence of a tetrahedral coordination environment at saturating levels of Co(II) (44, 45). These data indicate that InrS possesses a Ni(II) sensing site with analogy to NikR rather than RcnR, implying independent evolution of similar sensory motifs within distinct protein scaffolds suggestive of a limited, but relatively facile to evolve, repertoire of bioinorganic solutions that favor Ni(II). In turn, the metal site of the ArsR/SmtB family Ni(II) sensor NmtR has commonality with RcnR (55).

InrS possesses an N-terminal extension (relative to CsoR and RcnR) rich in His residues (supplemental Fig. S1). Similar extensions occur in several proteins of Ni(II) homeostasis and may aid Ni(II) acquisition from exchangeable cytosolic Ni(II) pools, a notable example being the hydrogenase assembly metallochaperone HypB from *Bradyrhizobium japonicum* (56). A mobile C-terminal metal binding region of NmtR may also act in this manner (55). Proteins related to InrS, with a similar ligand motif and/or deduced to regulate *nrsD*-like genes, form two clades (supplemental Fig. S13). Moreover, both clades are distinct from RcnR.

Each bacterium contains some complement of metal sensors from multiple families. Regardless of the molecular mechanism or family, the correct sensor in the set must respond to the correct metal. There are often inconsistencies in protein metal affinities measured in different studies (6, 57, 58), but here affinities of the tightest exchangeable site of *Synechocystis* sensors (InrS, ZiaR, CoaR, and Zur), representing four distinct sensor families, have been determined concurrently by common methods to discover that the *bona fide* Ni(II) sensor InrS does indeed have the tightest K_D Ni(II) of this set (Figs. 5 and 6 and supplemental Figs. S8 and S9). By controlling the buffered concentration of a metal in the cytosol each sensor has the capacity to influence the metals detected by other sensors in the same cell by maintaining a metal concentration below their binding constants. Thus, CoaR, Zur, and ZiaR may never bind Ni(II) *in vivo* and so fail to respond even if Ni(II) could otherwise trigger their allosteric mechanisms (supplemental Fig. S14). The metal sensors in each organism may thus have evolved as a set based, in part, upon their relative metal affinities (6). Inability of mycobacterial NmtR to detect Ni(II) in a cyanobacterial cytosol (27), and gain of Mn(II) detection by Fe(II)-sensing DtxR when transferred from *Corynebacterium diphtheria* to *B. subtilis* (59), are explained by such a model.

Metal affinities are a function of metal exchange via free solution, yet it is anticipated that the cytosol contains negligible hexa-aqua Ni(II). For example, if Ni(II) were buffered to 2×10^{-14} M (noting that the cell is expected to depart from thermodynamic equilibrium) a free Ni(II) atom would only occur in one cell in 100,000, or in each cell for a 1/100,000 of the time (assuming that one atom/cell volume approximates nanomolar) (60). Associative metal exchange is expected to occur *in vivo* via the polydisperse buffer of the cytosol. The K_D values (Fig. 6*I*) will correctly rank the sensors' preferences for Ni(II) *in vivo* if (as an initial approximation) their rates of exchange with cytosolic ligands retain the same rank order, but crucially the reported K_D values will not be indicative of *in vivo* kinetics.

Hydrogenase is Ni(II)-limited in many cyanobacteria (28–32), and in *Synechocystis* this enzyme dissipates surplus products of photosynthesis. Mutants without InrS have depleted Ni(II) content (Fig. 4*A*), and so hydrogenase is speculated to be even less active. An increase in protective pigments is predicted to dampen the light reactions of photosynthesis and hence to lessen demand for hydrogenase activity, which is consistent with the observed decline in chlorophyll *a* fluorescence in Δ*inrS* (Fig. 4, *B–D*). Conversely, and tantalizingly, allosterically competent InrS variants with weaker K_D Ni(II) should maintain an elevated cytosolic [Ni(II)] and sus-

tain greater rates of hydrogen evolution. In this way, metal sensors may be exploited to engineer metal supply for useful chemical transformations.

REFERENCES

1. Keren, N., Aurora, R., and Pakrasi, H. B. (2004) Critical roles of bacterioferritins in iron storage and proliferation of cyanobacteria. *Plant Physiol.* **135,** 1666–1673
2. So, A. K., and Espie, G. S. (1998) Cloning, characterization and expression of carbonic anhydrase from the cyanobacterium *Synechocystis* PCC6803. *Plant Mol. Biol.* **37,** 205–215
3. Tottey, S., Harvie, D. R., and Robinson, N. J. (2007) *Microbiol. Monogr.* **6,** 3–35
4. Appel, J., Phunpruch, S., Steinmüller, K., and Schulz, R. (2000) The bidirectional hydrogenase of *Synechocystis* sp. PCC 6803 works as an electron valve during photosynthesis. *Arch. Microbiol.* **173,** 333–338
5. Savage, N. (2011) Algae: the scum solution. *Nature* **474,** S15–16
6. Waldron, K. J., and Robinson, N. J. (2009) How do bacterial cells ensure that metalloproteins get the correct metal? *Nat. Rev. Microbiol.* **7,** 25–35
7. Waldron, K. J., Rutherford, J. C., Ford, D., and Robinson, N. J. (2009) Metalloproteins and metal sensing. *Nature* **460,** 823–830
8. Liu, T., Ramesh, A., Ma, Z., Ward, S. K., Zhang, L., George, G. N., Talaat, A. M., Sacchettini, J. C., and Giedroc, D. P. (2007) CsoR is a novel *Mycobacterium tuberculosis* copper-sensing transcriptional regulator. *Nat. Chem. Biol.* **3,** 60–68
9. Iwig, J. S., Rowe, J. L., and Chivers, P. T. (2006) Nickel homeostasis in *Escherichia coli*: the rcnR-rcnA efflux pathway and its linkage to NikR function. *Mol. Microbiol.* **62,** 252–262
10. Iwig, J. S., Leitch, S., Herbst, R. W., Maroney, M. J., and Chivers, P. T. (2008) Ni(II) and Co(II) sensing by *Escherichia coli* RcnR. *J. Am. Chem. Soc.* **130,** 7592–7606
11. Smaldone, G. T., and Helmann, J. D. (2007) CsoR regulates the copper efflux operon copZA in *Bacillus subtilis*. *Microbiology* **153,** 4123–4128
12. Ma, Z., Cowart, D. M., Scott, R. A., and Giedroc, D. P. (2009) Molecular insights into the metal selectivity of the copper(I)-sensing repressor CsoR from *Bacillus subtilis*. *Biochemistry* **48,** 3325–3334
13. Corbett, D., Schuler, S., Glenn, S., Andrew, P. W., Cavet, J. S., and Roberts, I. S. (2011) The combined actions of the copper-responsive repressor CsoR and copper-metallochaperone CopZ modulate CopA-mediated copper efflux in the intracellular pathogen *Listeria monocytogenes*. *Mol. Microbiol.* **81,** 457–472
14. Sakamoto, K., Agari, Y., Agari, K., Kuramitsu, S., and Shinkai, A. (2010) Structural and functional characterization of the transcriptional repressor CsoR from *Thermus thermophilus* HB8. *Microbiology* **156,** 1993–2005
15. Grossoehme, N., Kehl-Fie, T. E., Ma, Z., Adams, K. W., Cowart, D. M., Scott, R. A., Skaar, E. P., and Giedroc, D. P. (2011) Control of copper resistance and inorganic sulfur metabolism by paralogous regulators in *Staphylococcus aureus*. *J. Biol. Chem.* **286,** 13522–13531
16. Baker, J., Sengupta, M., Jayaswal, R. K., and Morrissey, J. A. (2011) The *Staphylococcus aureus* CsoR regulates both chromosomal and plasmid-encoded copper resistance mechanisms. *Environ. Microbiol.* **13,** 2495–2507
17. Festa, R. A., Jones, M. B., Butler-Wu, S., Sinsimer, D., Gerads, R., Bishai, W. R., Peterson, S. N., and Darwin, K. H. (2011) A novel copper-responsive regulon in *Mycobacterium tuberculosis*. *Mol. Microbiol.* **79,** 133–148
18. Zhu, T., Tian, J., Zhang, S., Wu, N., and Fan, Y. (2011) Identification of the transcriptional regulator NcrB in the nickel resistance determinant of *Leptospirillum ferriphilum* UBK03. *PLoS One* **6,** e17367
19. Ma, Z., Cowart, D. M., Ward, B. P., Arnold R. J., DiMarchi, R. D., Zhang, L., George, G. N., Scott, R. A., and Giedroc, D. P. (2009) Unnatural amino acid substitution as a probe of the allosteric coupling pathway in a mycobacterial Cu(I) sensor. *J. Am. Chem. Soc.* **131,** 18044–18045
20. Ma, Z., Jacobsen, F. E., and Giedroc, D. P. (2009) Coordination chemistry of bacterial metal transport and sensing. *Chem. Rev.* **109,** 4644–4681
21. Tottey, S., Rich, P. R., Rondet, S. A., and Robinson, N. J. (2001) Two Menkes-type ATPases supply copper for photosynthesis in *Synechocystis* PCC 6803. *J. Biol. Chem.* **276,** 19999–20004
22. Wood, P. M. (1978) Interchangeable copper and iron proteins in algal photosynthesis: studies on plastocyanin and cytochrome c_{552} in *Chlamydomonas*. *Eur. J. Biochem.* **87,** 9–19
23. Merchant, S., Hill, K., and Howe, G. (1991) Dynamic interplay between two copper-titrating components in the transcriptional regulation of Cyt c_6. *EMBO J.* **10,** 1383–1389
24. Quinn, J. M., Eriksson, M., Moseley, J. L., and Merchant, S. (2002) Oxygen deficiency-responsive gene expression in *Chlamydomonas reinhardtii* through a copper-sensing signal transduction pathway. *Plant Physiol.* **128,** 463–471
25. García-Domínguez, M., Lopez-Maury, L., Florencio, F. J., and Reyes, J. C. (2000) A gene cluster involved in metal homeostasis in the cyanobacterium *Synechocystis* sp. strain PCC 6803. *J. Bacteriol.* **182,** 1507–1514
26. López-Maury, L., García-Domínguez, M., Florencio, F. J., and Reyes, J. C. (2002) A two-component signal transduction system involved in nickel sensing in the cyanobacterium *Synechocystis* sp. PCC 6803. *Mol. Microbiol.* **43,** 247–256
27. Cavet, J. S., Meng, W., Pennella, M. A., Appelhoff, R. J., Giedroc, D. P., and Robinson, N. J. (2002) A nickel-cobalt-sensing ArsR-SmtB family repressor: contributions of cytosol and effector binding sites to metal selectivity. *J. Biol. Chem.* **277,** 38441–38448
28. Xiankong, Z., Tabita, R., and vanBaalen, C. (1984) Nickel control of hydrogen production and uptake in *Anabaena* spp. strains CA and 1F. *J. Gen. Microbiol.* **130,** 1815–1818
29. Daday, A., Mackerras, A. H., and Smith, G. D. (1985) Effect of nickel on hydrogen metabolism and nitrogen fixation in the *Cyanobacterium Anabaena cylindrica*. *J. Gen. Microbiol.* **131,** 231–238
30. Kumar, S., and Polasa, H. (1991) *Proc. Ind. Natl. Sci. Acad.* **1357,** 281–285
31. Oxelfelt, F., Tamagnini, P., Salema, R., and Lindblad, P. (1995) *Plant. Physiol. Biochem.* **33,** 617–623
32. Axelsson, R., and Lindblad, P. (2002) Transcriptional regulation of Nostoc hydrogenases: effects of oxygen, hydrogen, and nickel. *Appl. Environ. Microbiol.* **68,** 444–447
33. Rutherford, J. C., Cavet, J. S., and Robinson, N. J. (1999) Cobalt-dependent transcriptional switching by a dual-effector MerR-like protein regulates a cobalt-exporting variant CPx-type ATPase. *J. Biol. Chem.* **274,** 25827–25832
34. Thelwell, C., Robinson, N. J., and Turner-Cavet, J. S. (1998) An SmtB-like repressor from *Synechocystis* PCC 6803 regulates a zinc exporter. *Proc. Natl. Acad. Sci. U.S.A.* **95,** 10728–10733
35. Pakrasi, H. B., Ogawa, T., and Bhattacharyya-Pakrasi, M. (2004) *Transport of Metals: A Key Process in Oxygenic Photosynthesis* in *Regulatory Aspects of Photosynthesis* (Aro, E.-M., and Andersson, B., eds) pp. 253–264, Kluwer Academic, Dordrecht
36. Tottey, S., Patterson, C. J., Banci, L., Bertini, I., Felli, I. C., Pavelkova, A., Dainty, S. J., Pernil, R., Waldron, K. J., Foster, A. W., and Robinson, N. J. (2012) Cyanobacterial metallochaperone inhibits deleterious side reactions of copper. *Proc. Natl. Acad. Sci. U.S.A.* **109,** 95–100
37. Dainty, S. J., Patterson, C. J., Waldron, K. J., and Robinson, N. J. (2010) Interaction between cyanobacterial copper chaperone Atx1 and zinc homeostasis. *J. Biol. Inorg. Chem.* **15,** 77–85
38. Ellman, G. L. (1959) Tissue sulfhydryl groups. *Arch. Biochem. Biophys.* **82,** 70–77
39. Riddles, P. W., Blakeley, R. L., and Zerner, B. (1979) Ellman's reagent: 5,5′-dithiobis(2-nitrobenzoic acid), a reexamination. *Anal. Biochem.* **94,** 75–81
40. Huckle, J. W., Morby, A. P., Turner, J. S., and Robinson, N. J. (1993) Isolation of a prokaryotic metallothionein locus and analysis of transcriptional control by trace metal ions. *Mol. Microbiol.* **7,** 177–187
41. Sambrook, J., and Russell, D. W. (2001) *Molecular Cloning: A Laboratory Manual,* 3rd Ed., Cold Spring Harbor Laboratory, Cold Spring Harbor, NY
42. Wang, Q., Hall, C. L., Al-Adami, M. Z., and He, Q. (2010) IsiA is required for the formation of photosystem I supercomplexes and for efficient state transition in *Synechocystis* PCC 6803. *PLoS One* **5,** e10432
43. Golynskiy, M. V., Gunderson, W. A., Hendrich, M. P., and Cohen, S. M. (2006) Metal binding studies and EPR spectroscopy of the manganese transport regulator MntR. *Biochemistry* **45,** 15359–15372

44. VanZile, M. L., Cosper, N. J., Scott, R. A., and Giedroc, D. P. (2000) The zinc metalloregulatory protein *Synechococcus* PCC7942 SmtB binds a single zinc ion per monomer with high affinity in a tetrahedral coordination geometry. *Biochemistry* **39,** 11818–11829
45. Wang, S. C., Dias, A. V., Bloom, S. L., and Zamble, D. B. (2004) Selectivity of metal binding and metal-induced stability of *Escherichia coli* NikR. *Biochemistry* **43,** 10018–10028
46. Iwig, J. S., and Chivers, P. T. (2009) DNA recognition and wrapping by *Escherichia coli* RcnR. *J. Mol. Biol.* **393,** 514–526
47. Bullerjahn, G. S., and Sherman, L. A. (1986) Identification of a carotenoid-binding protein in the cytoplasmic membrane from the heterotrophic cyanobacterium *Synechocystis* sp. strain PCC6714. *J. Bact.* **167,** 396–399
48. Rakhimberdieva, M. G., Stadnichuk, I. N., Elanskaya, I. V., and Karapetyan, N. V. (2004) Carotenoid-induced quenching of the phycobilisome fluorescence in photosystem II-deficient mutant of *Synechocystis* sp. *FEBS Lett.* **574,** 85–88
49. Wilson, A., Ajlani, G., Verbavatz, J. M., Vass, I., Kerfeld, C. A., and Kirilovsky, D. (2006) A soluble carotenoid protein involved in phycobilisome-related energy dissipation in cyanobacteria. *Plant Cell* **18,** 992–1007
50. Odermatt, A., and Solioz, M. (1995) Two trans-acting metalloregulatory proteins controlling expression of the copper-ATPases of *Enterococcus hirae*. *J. Biol. Chem.* **270,** 4349–4354
51. Cobine, P. A., George, G. N., Jones, C. E., Wickramasinghe, W. A., Solioz, M., and Dameron, C. T. (2002) Copper transfer from the Cu(I) chaperone, CopZ, to the repressor, Zn(II)CopY: metal coordination environments and protein interactions. *Biochemistry* **41,** 5822–5829
52. Jenkins, R. M., Singleton, M. L., Almaraz, E., Reibenspies, J. H., and Darensbourg, M. Y. (2009) Imidazole-containing (N3S)-Ni(II) complexes relating to nickel-containing biomolecules. *Inorg. Chem.* **48,** 7280–7293
53. Vasák, M., Kägi, J. H., Holmquist, B., and Vallee, B. L. (1981) Spectral studies of cobalt (II)- and nickel (II)-metallothionein. *Biochemistry* **20,** 6659–6664
54. Ferris, N. S., Woodruff, W. H., Tennent, D. L., and McMillin, D. R. (1979) Native azurin and its Ni(II) derivative: a resonance Raman study. *Biochem. Biophys. Res. Commun.* **88,** 288–296
55. Reyes-Caballero, H., Lee, C. W., and Giedroc, D. P. (2011) *Mycobacterium tuberculosis* NmtR harbors a nickel sensing site with parallels to *Escherichia coli* RcnR. *Biochemistry* **50,** 7941–7952
56. Olson, J. W., Fu, C., and Maier, R. J. (1997) The HypB protein from *Bradyrhizobium japonicum* can store nickel and is required for the nickel-dependent transcriptional regulation of hydrogenase. *Mol. Microbiol.* **24,** 119–128
57. Xiao, Z., and Wedd, A. G. (2010) The challenges of determining metal-protein affinities. *Nat. Prod. Rep.* **27,** 768–789
58. Xiao, Z., Brose, J., Schimo, S., Ackland, S. M., La Fontaine, S., and Wedd, A. G. (2011) Unification of the copper(I) binding affinities of the metallochaperones Atx1, Atox1, and related proteins: detection probes and affinity standards. *J. Biol. Chem.* **286,** 11047–11055
59. Guedon, E., and Helmann, J. D. (2003) Origins of metal ion selectivity in the DtxR/MntR family of metalloregulators. *Mol. Microbiol.* **48,** 495–506
60. Changela, A., Chen, K., Xue, Y., Holschen, J., Outten, C. E., O'Halloran, T. V., and Mondragón, A. (2003) Molecular basis of metal-ion selectivity and zeptomolar sensitivity by CueR. *Science* **301,** 1383–1387